CHAPTER IV

RESULTS AND DISCUSSION

4.1 Investigation of Organoclays Dispersion Behavior in DMSO

Metal-containing polyurethanes, namely PB900Zn, PP1000Zn, PB1600Zn, PP2300Zn, PB900Ni, PP1000Ni, PB1600Ni and PP2300Ni, are soluble in $CHCl_3$, THF, CH_2Cl_2, DMF and DMSO as described in the literature [39]. The polymers show the best solubility in DMSO. Therefore, the organoclay employed for the preparation metal-containing polyurethane (PU)/organoclay nanocomposites should be able to disperse in DMSO. This experimental part is intended to find the most suitable organoclay for the preparation of metal-containing PU/organoclay nanocomposites.

Ngumnunjai [37] prepared different types of organoclays employing various surfactants with various amounts of surfactant loading. Three quaternary ammonium salts used as surfactants in the preparation of organoclay from bentonite H (BNH) were tallowtrimethyl ammonium chloride (TTM), oleylmethylbis(2-hydroxyethyl)ammonium chloride (OMH) and octadecylmethyl[ethoxylate(15)] ammonium chloride (ODMH) (Figure 4.1). The surfactants were dispersed in distilled water at various concentrations of 0.5, 1.0 and 1.5 mmol/g clay. After dispersion in DMSO, the organoclay/DMSO mixture showed different behavior as shown in Table 4.1 and Figure 4.2. It was found that the TTM-modified organoclay (TTM-BNH) at all concentrations, OMH-modified organoclay (OMH-BNH) at the concentrations of 0.5 and 1.0 mmol and ODMH-modified organoclay (ODMH-BNH) at the concentration of 0.5 mmol showed sedimentation in DMSO. The OMH-BNH at the concentration 1.5 mmol swelled in DMSO. The ODMH-BNH at the concentrations of 1.0 and 1.5 mmol showed suspension in DMSO. The dispersion behavior of organoclays in DMSO can be interpreted as follows:

(a) Sedimentation: this is the least desirable behavior since the organoclay surface is incompatible with the solvent.

(b) Swelling: this behavior is acceptable but not desirable since the organoclay surface is partially compatible with the solvent.

(c) Suspension: this is the most desirable condition since most of the organoclays are fully dispersed in the solvent.

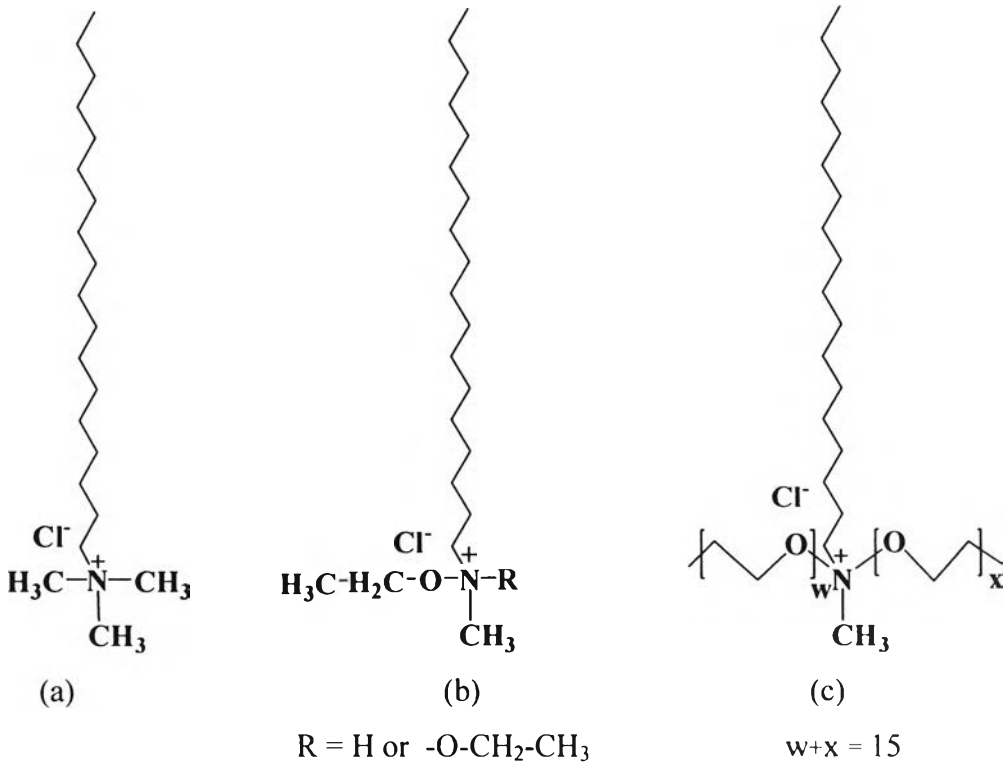

Figure 4.1 Structure of surfactants (a) TTM, (b) OMH and (c) ODMH

The appearance after the dispersion of OMH-BNH at the concentration 0.5 and 1.5 mmol and ODMH-BNH at the concentrations of 1.0 and 1.5 mmol in DMSO is shown in Figure 4.2.

Table 4.1 The appearance of organoclay/DMSO mixture

Organoclay	Concentration of surfactant	The appearance after dispersion of organoclay in DMSO
TTM-BNH	0.5	sedimentation
	1.0	sedimentation
	1.5	sedimentation
OMH-BNH	0.5	sedimentation
	1.0	sedimentation
	1.5	swelling
ODMH-BNH	0.5	sedimentation
	1.0	suspension
	1.5	suspension

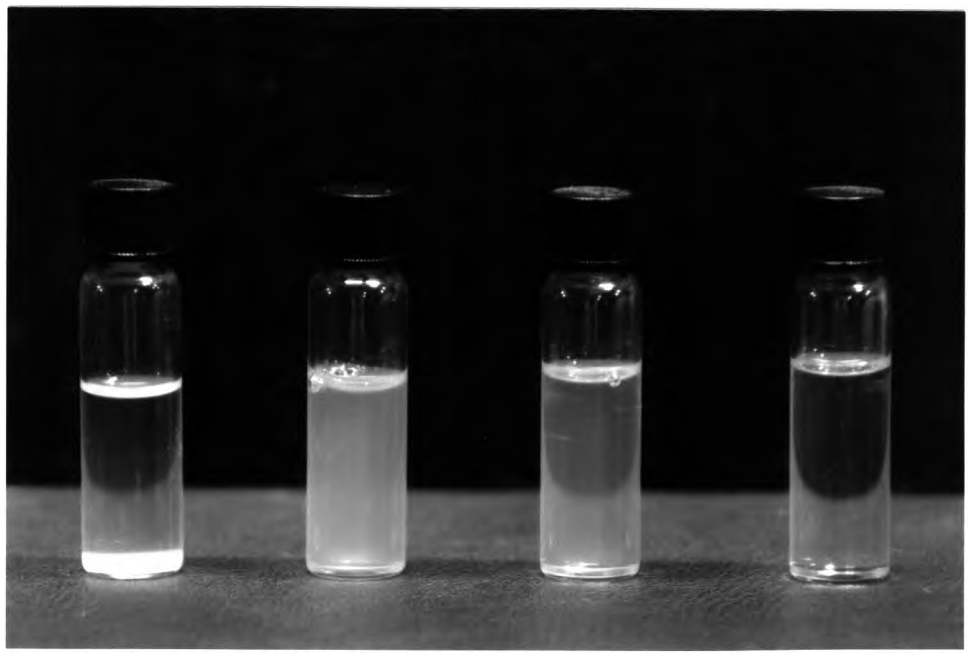

(a) **(b)** **(c)** **(d)**

Figure 4.2 The appearance of dispersed organoclay in DMSO (a) OMH-BNH 0.5 mmol (b) OMH-BNH 1.5 mmol (c) ODMH-BNH 1.0 mmol (d) ODMH-BNH 1.5 mmol

The above results indicated that OMH-BNH at the concentration of 1.5 mmol and ODMH-BNH at the concentrations 1.0 and 1.5 mmol are compatible with DMSO. Therefore, these organoclays were used in the preparation of metal-containing nanocomposite.

4.2 Preliminary Investigation of Metal-Containing Polyurethane/Organoclay Systems

The metal-containing polyurethane/organoclay system that was chosen for this study was PB900Zn/organoclay nanocomposites. Scheme 2.4 shows the preparation of PB900Zn polyurethane which was synthesized from $ZnSal_2$trien and PB900 prepolymer and Figure 2.5 shows an example of the preparation of PB900Zn/organoclay nanocomposites using PB900Zn polyurethane and OMH-BNH as an organoclay (PB900Zn/OMH-BNH). The organoclay content in PB900Zn/organoclay nanocomposites was 5 wt%.

The nanocomposite films were prepared and characterized by XRD. Figures 4.3-4.4 show XRD patterns of PB900Zn/OMH-BNH nanocomposite and its corresponding OMH-BNH organoclay at 0.5 and 1.5 mmol concentration, respectively. Figures 4.5-4.6 show XRD patterns of PB900Zn/ODMH-BNH nanocomposite and its corresponding ODMH-BNH organoclay at 1.0 and 1.5 mmol concentration, respectively. The XRD peak and the calculated d_{001} spacing of each nanocomposites are shown in Table 4.2.

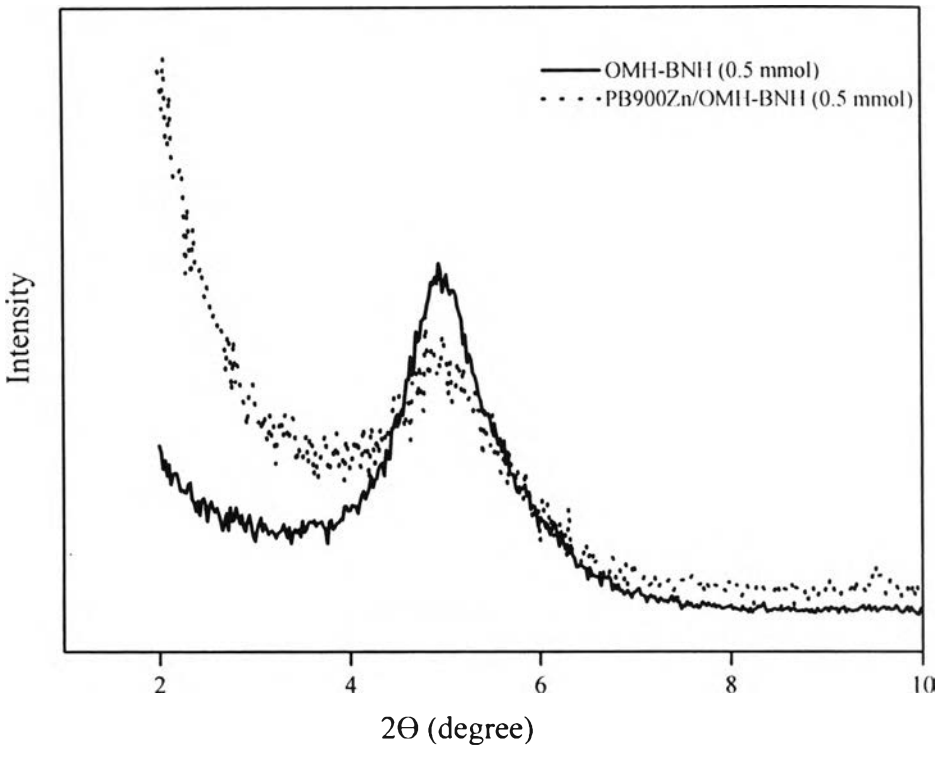

Figure 4.3 XRD patterns of PB900Zn/OMH-BNH nanocomposite and its corresponding OMH-BNH organoclay (0.5 mmol concentration)

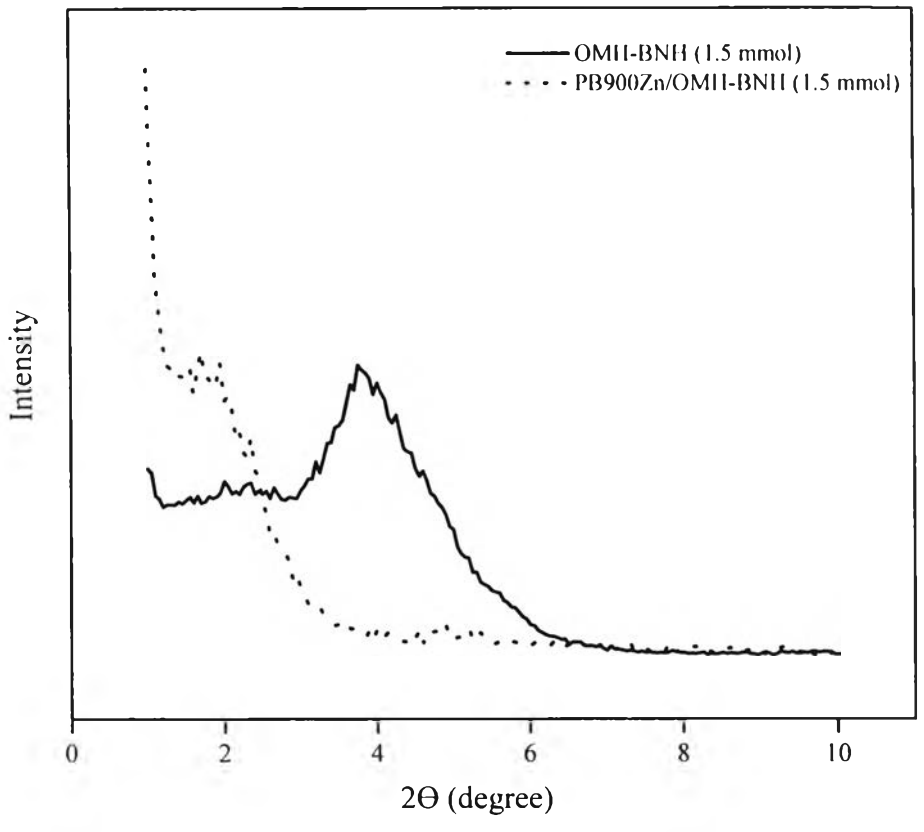

Figure 4.4 XRD patterns of PB900Zn/OMH-BNH nanocomposite and its corresponding OMH-BNH organoclay (1.5 mmol concentration)

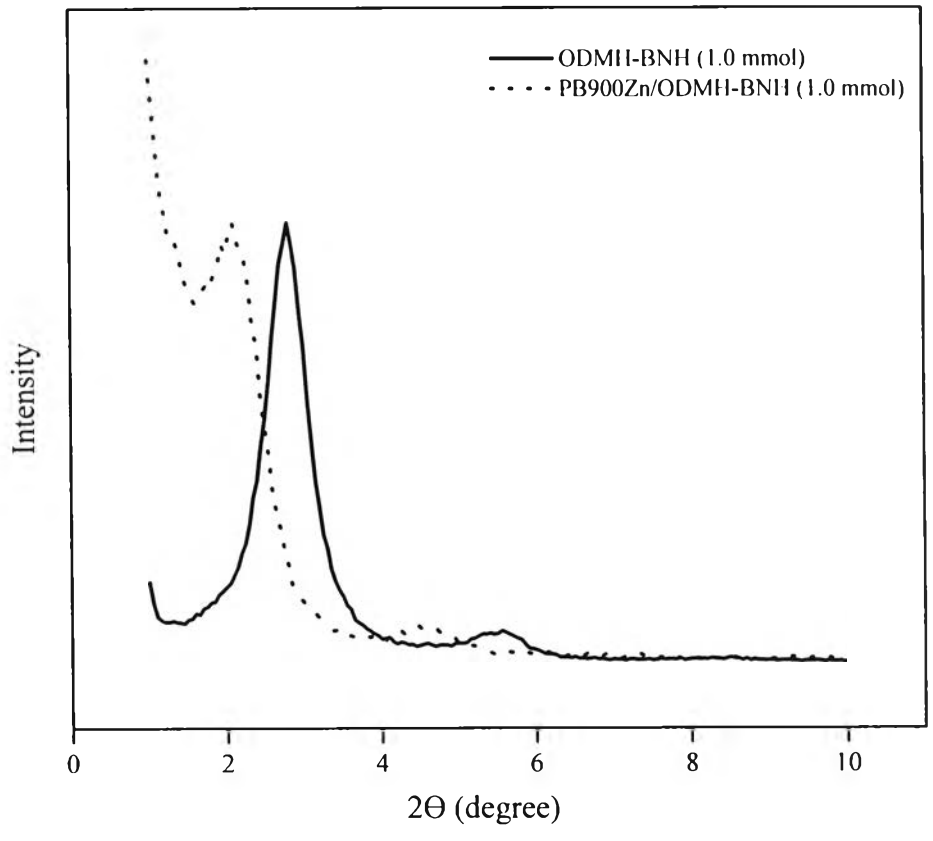

Figure 4.5 XRD patterns of PB900Zn/ODMH-BNH nanocomposite and its corresponding ODMH-BNH organoclay (1.0 mmol concentration)

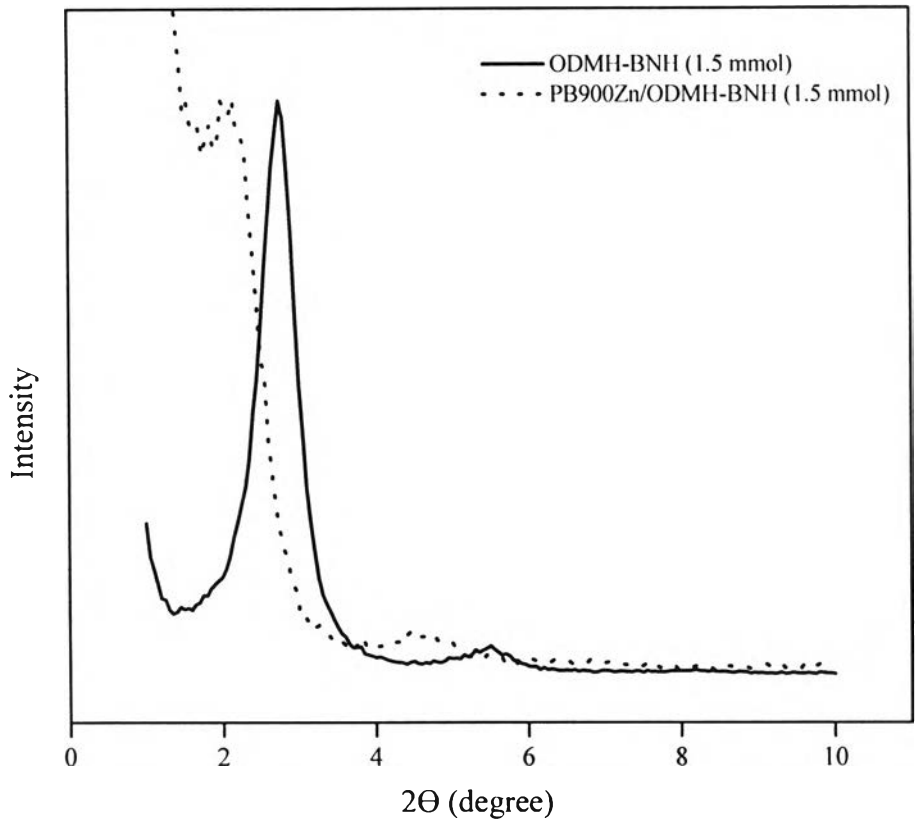

Figure 4.6 XRD patterns of PB900Zn/ODMH-BNH nanocomposite and its corresponding ODMH-BNH organoclay (1.5 mmol concentration)

Table 4.2 XRD data of OMH-BNH and ODMH-BNH organoclay and their corresponding nanocomposites

Organoclay and nanocomposite	d_{001} peak (2θ, degree)	Interlayer spacing (Å)	Different between interlayer spacing of organoclay and nanocomposite (Å)
OMH-BNH (0.5 mmol)	4.92	6.31	0
PB900Zn/OMH-BNH (0.5 mmol)	4.92	6.31	
OMH-BNH (1.5 mmol)	3.78	8.21	6.86
PB900Zn/OMH-BNH (1.5 mmol)	2.06	15.07	
ODMH-BNH (1.0 mmol)	2.79	11.12	3.66
PB900Zn/ODMH-BNH (1.0 mmol)	2.10	14.78	
ODMH-BNH (1.5 mmol)	2.78	11.16	3.55
PB900Zn/ODMH-BNH (1.5 mmol)	2.11	14.71	

The above data show that OMH-BNH organoclay (0.5 mmol), which sedimentation in DMSO is observed, has interlayer spacing (d-spacing) equals to its nanocomposite. Therefore, there is no intercalation of the polymer into the organoclay layer. In the cases of PB900Zn/OMH-BNH (1.5 mmol), PB900Zn/ODMH-BNH (1.0 mmol) and PB900/ODMH-BNH (1.5 mmol), the d-spacing of nanocomposites are higher than ones of their corresponding organoclays, which indicated that the organoclays were intercalated by the polymer. The OMH-BNH organoclay (1.5 mmol) and its corresponding nanocomposite showed the most different of d-spacing of 6.86 Å and this result suggested that the intercalated structure of nanocomposite should be clearly observed by the use of other analytical techniques, namely IR and TEM. Therefore, the OMH-BNH organoclay (1.5 mmol) was chosen for the preparation of nanocomposites. From this point, the terms "BNH" and "BNH organoclay" correspond to OMH-BNH organoclay (1.5 mmol) and its corresponding nanocomposite, respectively.

4.3 Preparation of Metal-Containing Polyurethane (PU)/BNH Nanocomposite Films

Having obtained a suitable BNH organoclay, eight metal-containing polyurethanes, namely PB900Zn, PP1000Zn, PB1600Zn, PP2300Zn, PB900Ni, PP1000Ni, PB1600Ni and PP2300Ni (Scheme 2.4) were then employed in the preparation of metal-containing polyurethanes/BNH organoclay nanocomposites.

The polymers were dissolved in DMSO to obtain the final concentration of the polymer in DMSO at 30 wt%, which is 2.0 g of polymer in 6.0 mL of DMSO. All metal-containing PU are soluble in DMSO except PB1600Ni and PP2300Ni which are partially soluble although the concentration of metal-containing PU solution was decreased to 5 wt%. Therefore, these metal-containing PU could not be used in the preparation of nanocomposites.

At room temperature, the solution of organoclay (1 wt% of BNH organoclay in 2.0 mL of DMSO) was added to the polymer and the mixture was stirred for 1 hour. The mixture was immediately cast onto a petridishes and DMSO was removed by use of a vacuum oven to obtain dried film. The temperature and time of drying nanocomposite in a vacuum oven to obtain suitable nanocomposite film for further characterization was varied between 40-80°C and 1-72 hours, respectively. The appearance of nanocomposites is shown in Tables 4.3 and 4.4.

After removal of DMSO, the obtained PB900Zn/BNH and PP1000Zn/BNH films had smooth surface and could be peeled off the petri dishes. The most suitable condition to obtain dried nanocomposite films was dried in vacuum oven at 50°C for 24 hours. The PB1600Zn/BNH and PP2300Zn/BNH films had smooth surface, however, the films were not completely dried and therefore the films were broken upon peeling from the petri dishes. For PB900Ni/BNH and PP1000Ni/BNH nanocomposites, the films could not be completely dried, although the drying temperature and time was increased to 80 °C for 72 hours. The agglomeration was observed and the films could not be removed from the petri dishes.

Table 4.3 The appearance of PB900Zn/BNH and PP1000Zn/BNH nanocomposite films after drying in a vacuum oven at different conditions

Appearance of nanocomposite films	Time (hours)				
	40 °C	50 °C	60 °C	70 °C	80 °C
Liquid mixture	1	1	1	1	1
Viscous mixture	8	6	6	4	5
Nearly dried film	18	14	13	12	12
Completely dried films and can be peeled off the petri dishes	30	24	24	23	22

Table 4.4 The appearance of PB900Ni/BNH, PP1000Ni/BNH, PB1600Zn/BNH and PP2300Zn/BNH nanocomposite films after drying in a vacuum oven at different conditions

Appearance of nanocomposite films	Time (hours)				
	40 °C	50 °C	60 °C	70 °C	80 °C
Liquid mixture	1	1	1	1	1
Viscous mixture	16	12	11	10	10
Nearly dried film	27	25	24	22	22
Completely dried films and can be peeled off the petri dishes	Not obtained				

PB900Zn/BNH and PP1000Zn/BNH were characterized by FTIR, XRD and TEM and thermal properties were investigated by TGA and measuring LOI. PB1600Zn/BNH, PP2300Zn/BNH, PB900Ni/BNH and PP1000Ni/BNH were characterized only by FTIR since the nanocomposite could not be obtained as film.

4.4 Characterization of Metal-Containing PU/BNH Nanocomposite Films

4.4.1 FTIR

FTIR spectroscopy can be used to investigate the chemical characteristics of the nanocomposite thin films. The IR data of metal-containing polyurethanes are shown in Table 4.5 [39].

Table 4.5 IR data of metal-containing polyurethanes

Polymer code	Wavenumber (cm^{-1})					
	NH_2	C=O	C=N	Phenyl ring		
PB900Zn	3440-3310	1720	1635	1600	1536	763
PP1000Zn	3440-3311	1729	1635	1600	1536	763
PB1600Zn	3440-3310	1720	1635	1600	1536	758
PB2300Zn	3440-3312	1724	1630	1600	1536	763
PB900Ni	3440-3314	1720	1640	1600	1536	758
PP1000Ni	3440-3315	1720	1635	1600	1536	758
PB1600Ni	3440-3315	1720	1640	1600	1536	756
PB2300Ni	3440-3317	1724	1635	1600	1536	758

An imine (C=N) stretching band from $MSal_2trien$ metal complex occurred at 1635 cm^{-1}. The carbonyl bands (C=O) due to the formation of a urethane linkage and urea linkage (-NCON-) were observed at 1726 cm^{-1} but the urea linkage peak was not clearly observed because peak of urethane linkage in the polymer overlapped with the urea linkage peak.

IR spectrum of BNH organoclay after surface modification with 1.5 mmol of OMH is shown in Figure 4.7 [37]. The peak at 3624, 3422, 2929, 2857, 1469, 1038, 519 and 459 cm^{-1} can be assigned as the O-H stretching of BNH, O-OH stretching of BNH, C-H stretching of methyl group, C-H stretching of methylene group, CH_3 deformation, Si-O stretching, Al-O stretching and Si-O bending, respectively. The characteristic peak of the surfactant at 2929, 2857 and 1469 cm^{-1} was observed in

organoclay but not observed in Na-BNH. The Na-BNH shows its characteristic peak at 3628, 3434, 1037, 522 and 465 cm^{-1} which are associated with O-H stretching, O-OH stretching, Si-O stretching, Al-O stretching and Si-bending, respectively. This result implies the success of the modification of Na-BNH.

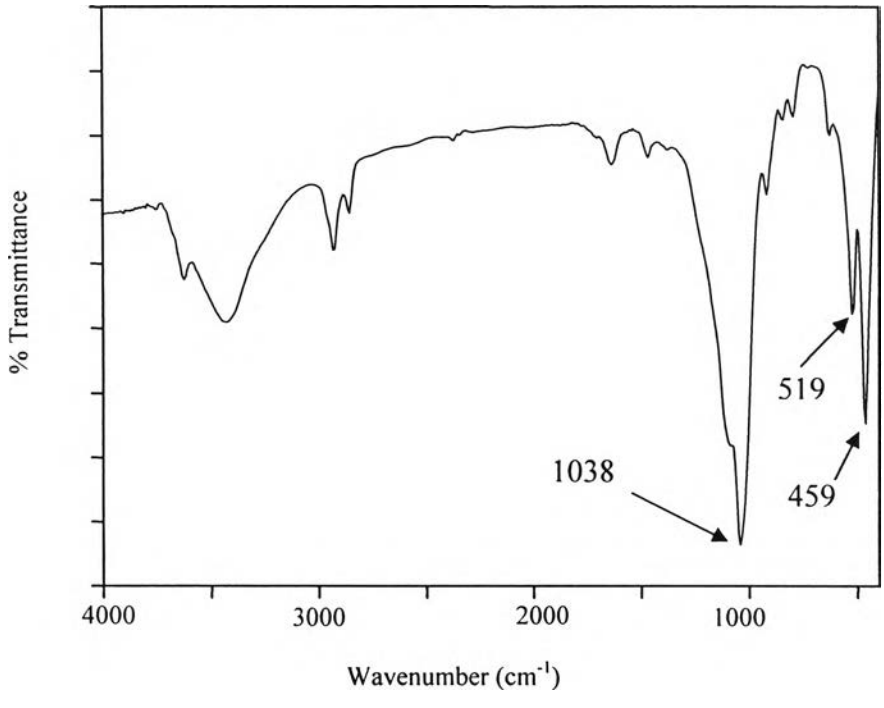

Figure 4.7 FTIR spectrum of BNH organoclay modified by 1.5 mmol OMH

FTIR spectra of BNH organoclay, metal-containing PU, namely PB900Zn, PP1000Zn, PB1600Zn, PP2300Zn, PB900Ni and PP1000Ni, and their corresponding metal-containing PU/BNH nanocomposite, namely PB900Zn/BNH, PP1000Zn/BNH, PB1600ZnBNH, PP2300Zn/BNH, PB900Ni/BNH and PP1000Ni/BNH, with various of organoclay contents of 1, 3 and 5 wt% in the nanocomposite are shown in Figures 4.8 - 4.13.

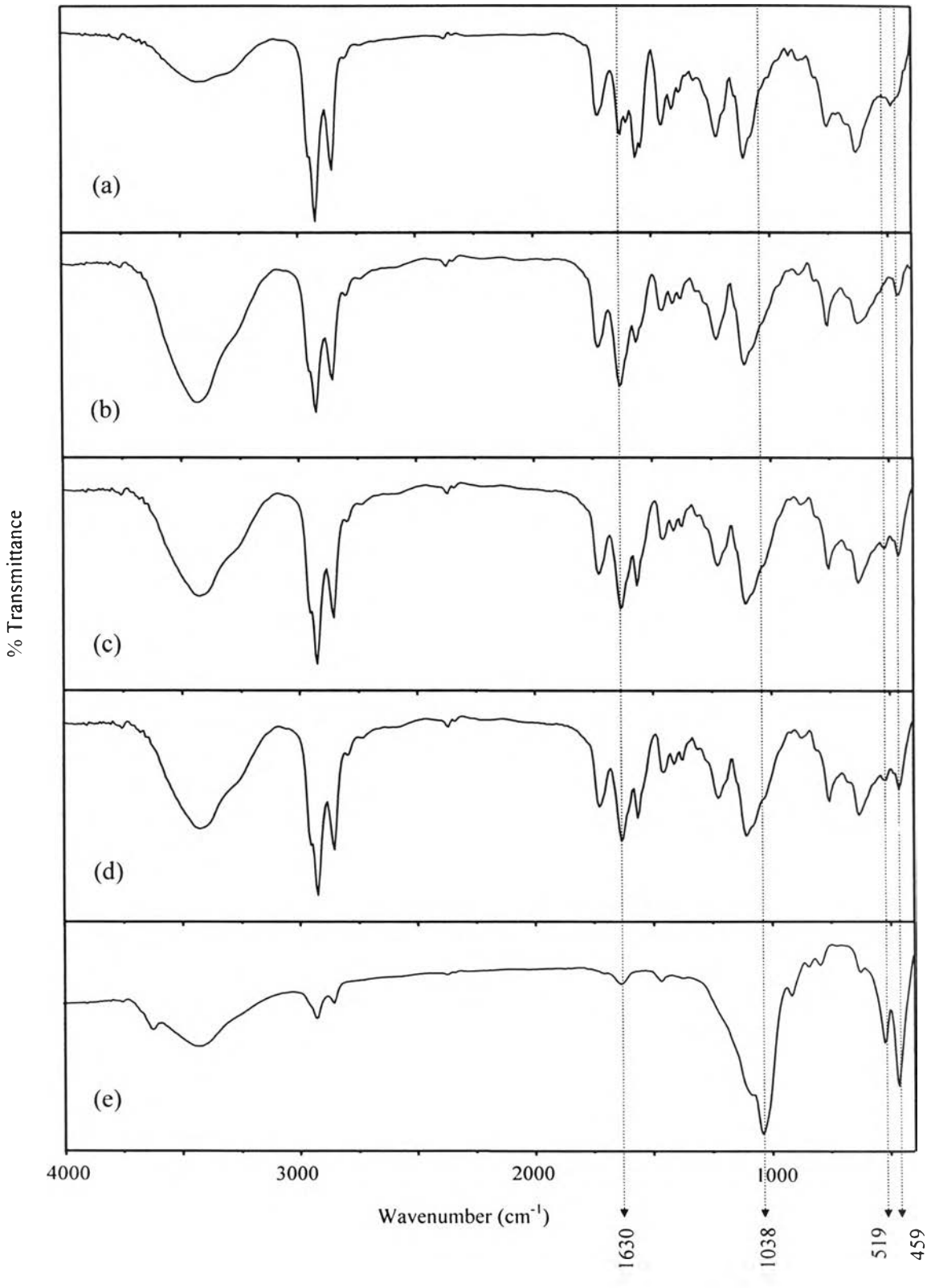

Figure 4.8 FTIR spectrum of (a) PB900Zn polyurethane (b) PB900Zn/BNH (1 wt%) (c) PB900Zn/BNH (3 wt%) (d) PB900Zn/BNH (5 wt%) (e) BNH organoclay

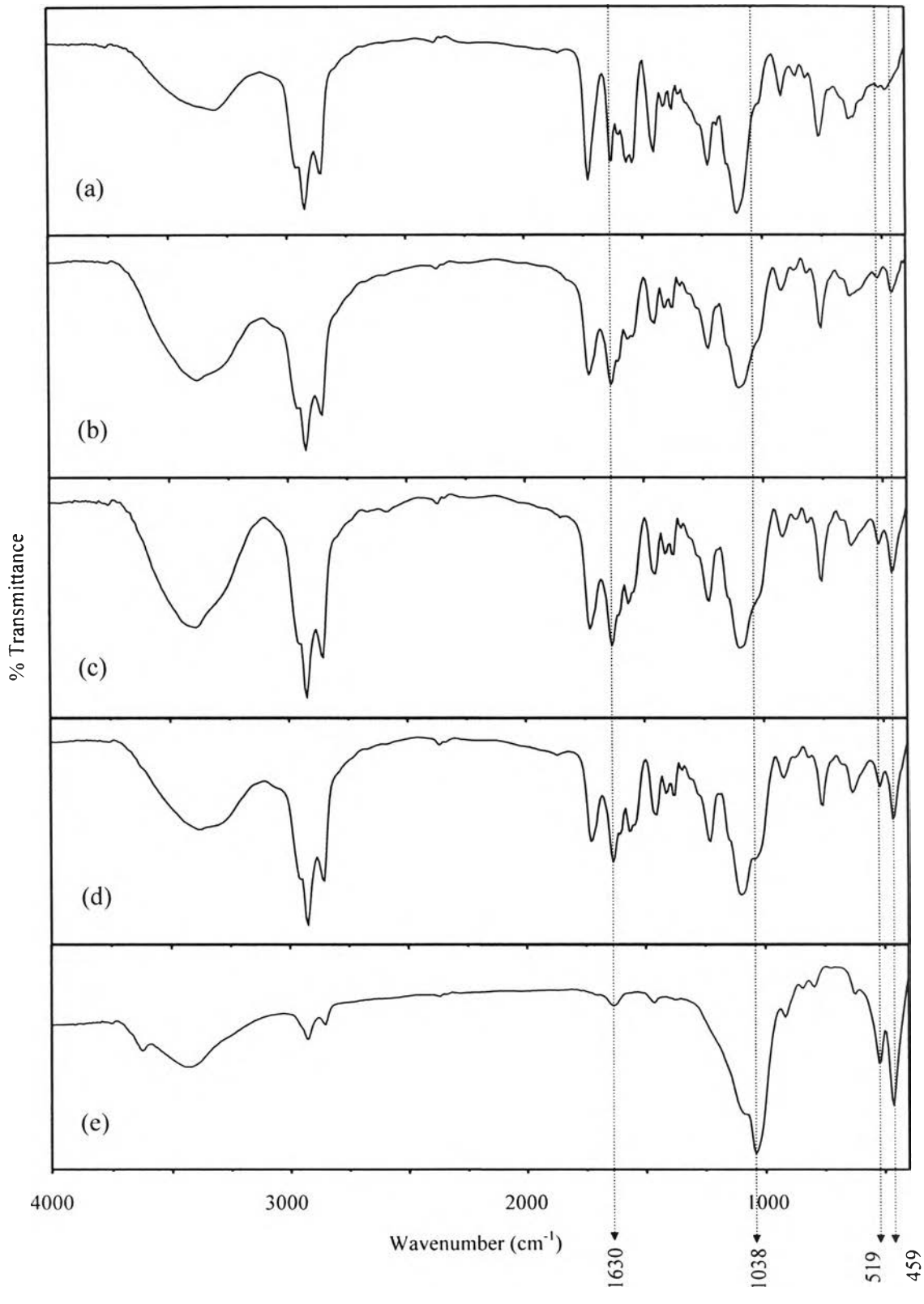

Figure 4.9 FTIR spectrum of (a) PP1000Zn polyurethane (b) PP1000Zn/BNH (1 wt%) (c) PP1000Zn/BNH (3 wt%) (d) PP1000Zn/BNH (5 wt%) (e) BNH organoclay

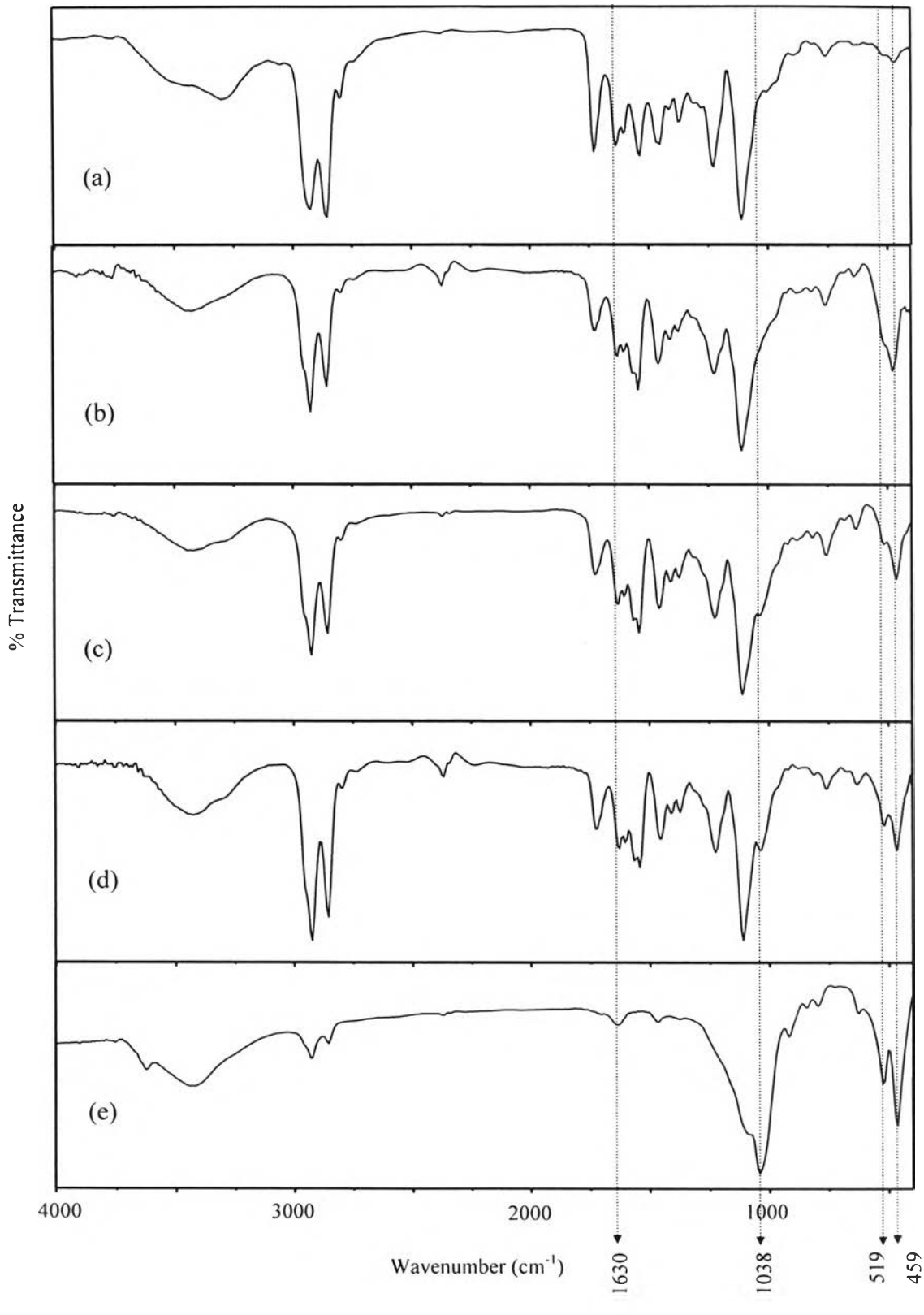

Figure 4.10 FTIR spectrum of (a) PB1600Zn polyurethane (b) PB1600Zn/BNH (1 wt%) (c) PB1600Zn/BNH (3 wt%) (d) PB1600Zn/BNH (5 wt%) (e) BNH organoclay

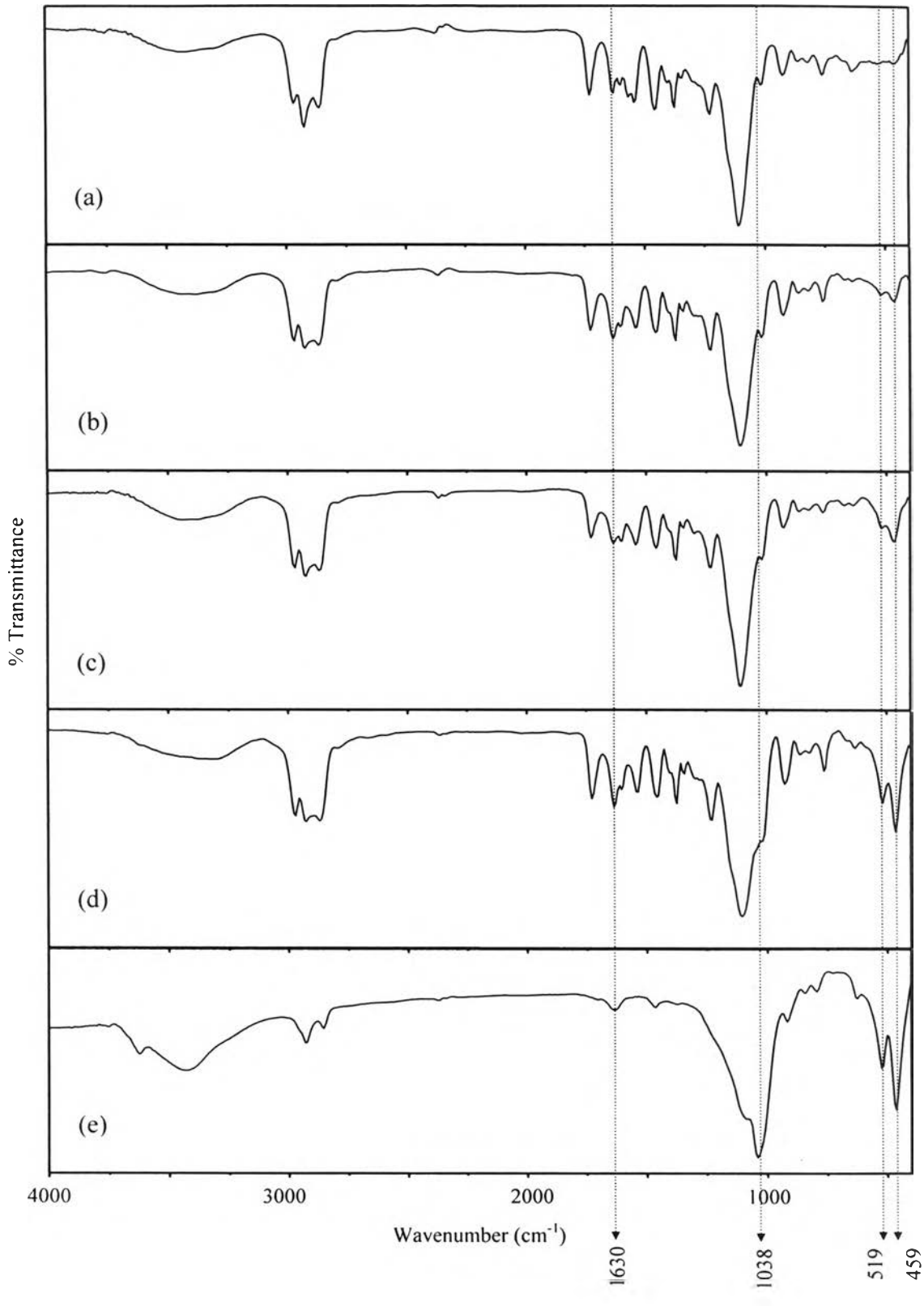

Figure 4.11 FTIR spectrum of (a) PP2300Zn polyurethane (b) PP2300Zn/BNH (1 wt%) (c) PP2300Zn/BNH (3 wt%) (d) PP2300Zn/BNH (5 wt%) (e) BNH organoclay

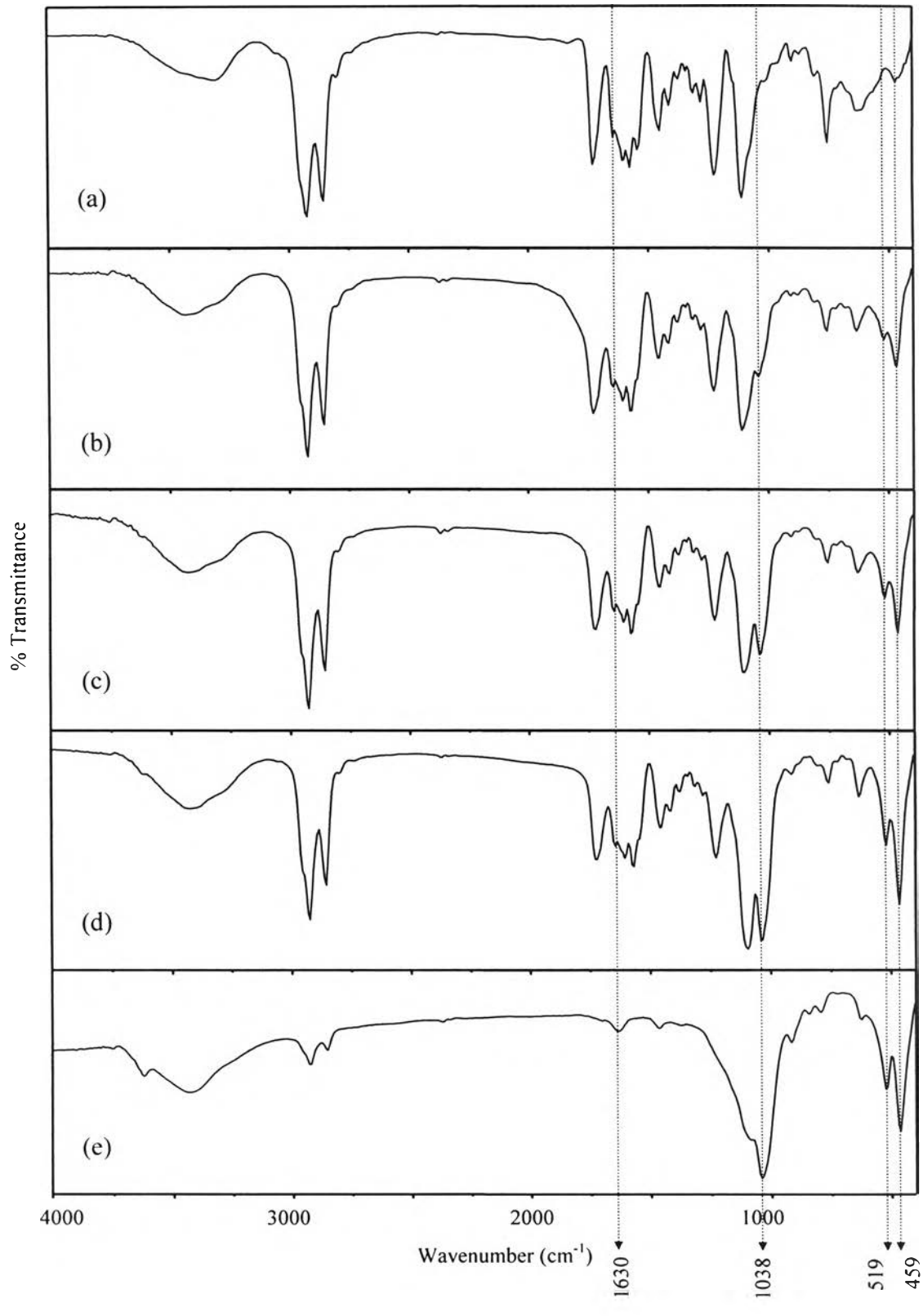

Figure 4.12 FTIR spectrum of (a) PB900Ni polyurethane (b) PB900Ni/BNH (1 wt%) (c) PB900Ni/BNH (3 wt%) (d) PB900Ni/BNH (5 wt%) (e) BNH organoclay

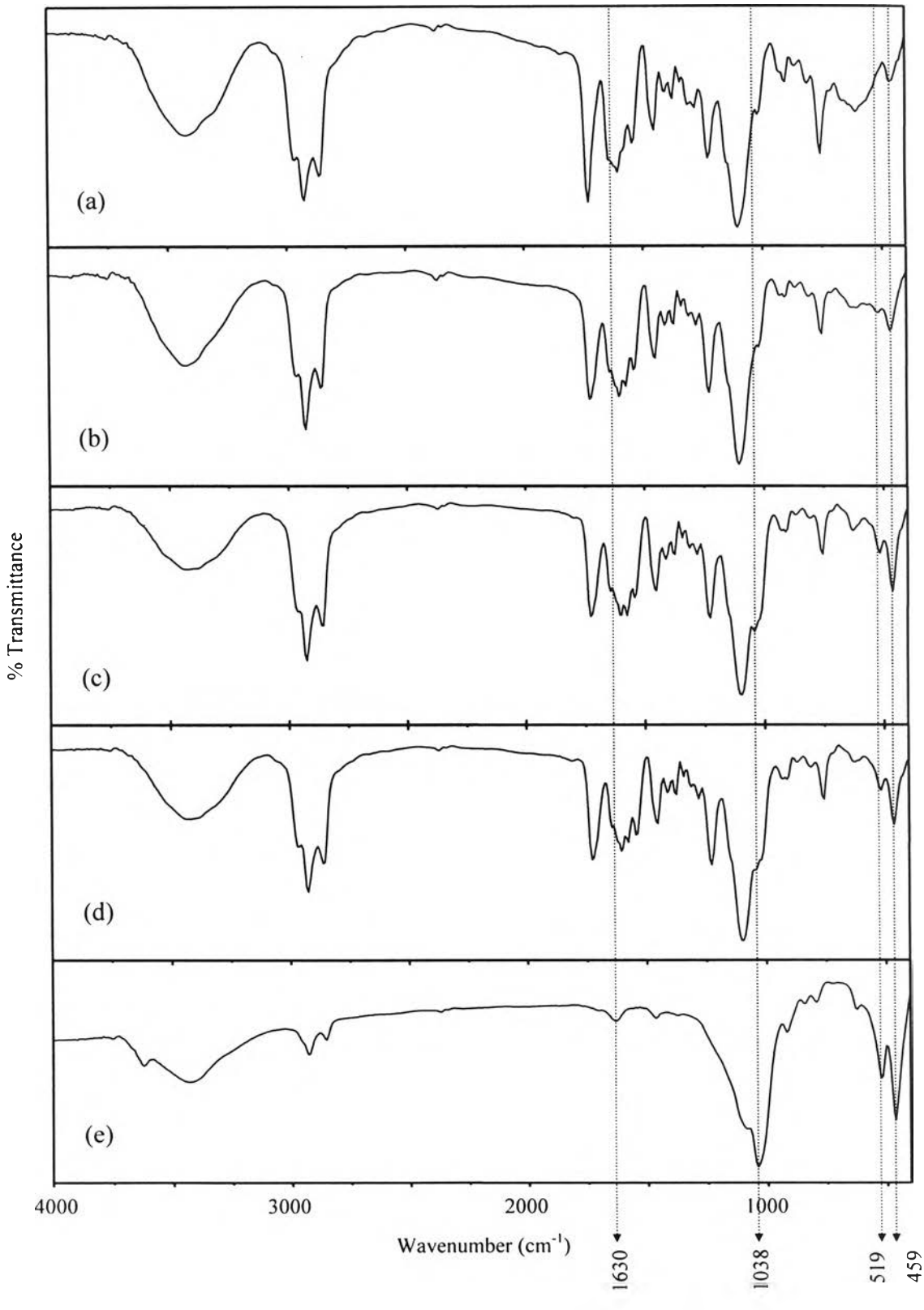

Figure 4.13 FTIR spectrum of (a) PP1000Ni polyurethane (b) PP1000Ni/BNH (1 wt%) (c) PP1000Ni/BNH (3 wt%) (d) PP1000Ni/BNH (5 wt%) (e) BNH organoclay

For PB900Zn/BNH and PP1000Zn/BNH nanocomposites, their FTIR spectra (Figures 4.8 and 4.9) showed a strong broad peak at 1630 cm^{-1}, which could also be observed in both PB900Zn and PP1000Zn polyurethanes. This peak was due to the overlapped peaks of C=N stretching and C=C phenyl ring of metal-containing polyurethanes. Comparing between the polymer and nanocomposite spectra, there was a change in the peak pattern around 1630 cm^{-1}, which was probably due to the interaction between the polymer and organoclay.

For PB900Zn/BNH, PP1000Zn/BNH, PB1600Zn/BNH, PP2300Zn/BNH, PB900Ni/BNH and PP1000Ni/BNH nanocomposites, the characteristic peaks of BNH organoclay at 1038, 519 and 459 cm^{-1} were observed, which could be assigned to Si-O stretching, Al-O stretching and Si-O bending, respectively. The intensity of all of these peaks increased with increasing organoclay content in the nanocomposite.

This indicates that BNH was incorporated with PB900Zn and PP1000Zn to yield nanocomposites and the chemical structure of the polymers was not changed by the presence of organoclay.

For PB1600Zn/BNH, PP2300Zn/BNH, PB900Ni/BNH and PP1000Ni/BNH (Figures 4.10-4.13), there was no change in the peak pattern at 1630 cm^{-1} and the characteristic peak of organoclay at 1038 cm^{-1} was not clearly observed in the nanocomposite spectra. This suggested that there was no interaction between organoclay and the polymers.

Moreover, PB900Zn/BNH and PP1000Zn/BNH nanocomposites showed broad peak at 1038 cm^{-1}, which suggested that there was an interaction between BNH organoclay and polymer chain to yield nanocomposites and the chemical structure of the polymers was not changed by the presence of organoclay. However, the PB1600Zn/BNH, PP2300Zn/BNH, PB900Ni/BNH and PP1000Ni/BNH nanocomposites showed sharp peak at this 1038 cm^{-1} position and this result suggested that there was less interaction between organoclay and polymer chain when compared to PB900Zn/BNH and PP1000Zn/BNH nanocomposites.

4.4.2 XRD

Two nanocomposites, PB900Zn/BNH and PP1000Zn/BNH, which could be obtained as film and showed good IR result, were then characterized by XRD and TEM. The XRD patterns of BNH organoclay, pure metal-containing PU and the metal-containing PU/BNH nanocomposites with different clay contents are shown in Figures 4.14-4.15. BNH organoclay showed a strong diffraction peak at $2\theta = 4.18^{o}$, corresponding to the d_{001} plane. According to Bragg's equation, the basal spacing is equal to 21.15 Å. All the XRD diffractogram of nanocomposites exhibited a diffraction peak of d_{001} corresponding to the regular interlayer spacing of the organosilicate platelets. Moreover, the d_{002}, d_{003} and d_{004} of this structure were also visible (Tables 4.6-4.9). The $d_{001\text{-ave}}$ means a diffraction peak average, which was calculated from d_{001}, d_{002}, d_{003} and d_{004}. From Figure 4.14, it can be seen that the $d_{001\text{-ave}}$ peak of BNH organoclay in PB900Zn/BNH nanocomposites shifted from $2\theta = 4.18^{o}$ to a lower angle of $2\theta = 2.42^{o}$. This indicated an increase in the interlayer distance from 21.1 to 36.5 Å. An increase in the interlayer spacing is usually indicative of an intercalated structure of alternating polymer and silicate layers. Moreover, the relative peak intensity increased with increasing in clay content.

Similar results were observed for the PP1000/BNH nanocomposite as shown in Figure 4.15. The $d_{001\text{-ave}}$ diffraction peak of BNH organoclay shifted from $2\theta = 4.18^{o}$ to $2\theta = 2.44^{o}$, which indicated that the interlayer distance of the clay increased from 21.1 to 36.2 Å. The relative peak intensity increased with increasing in clay content. These results also showed that the PU molecules intercalated into interlayer of the clay.

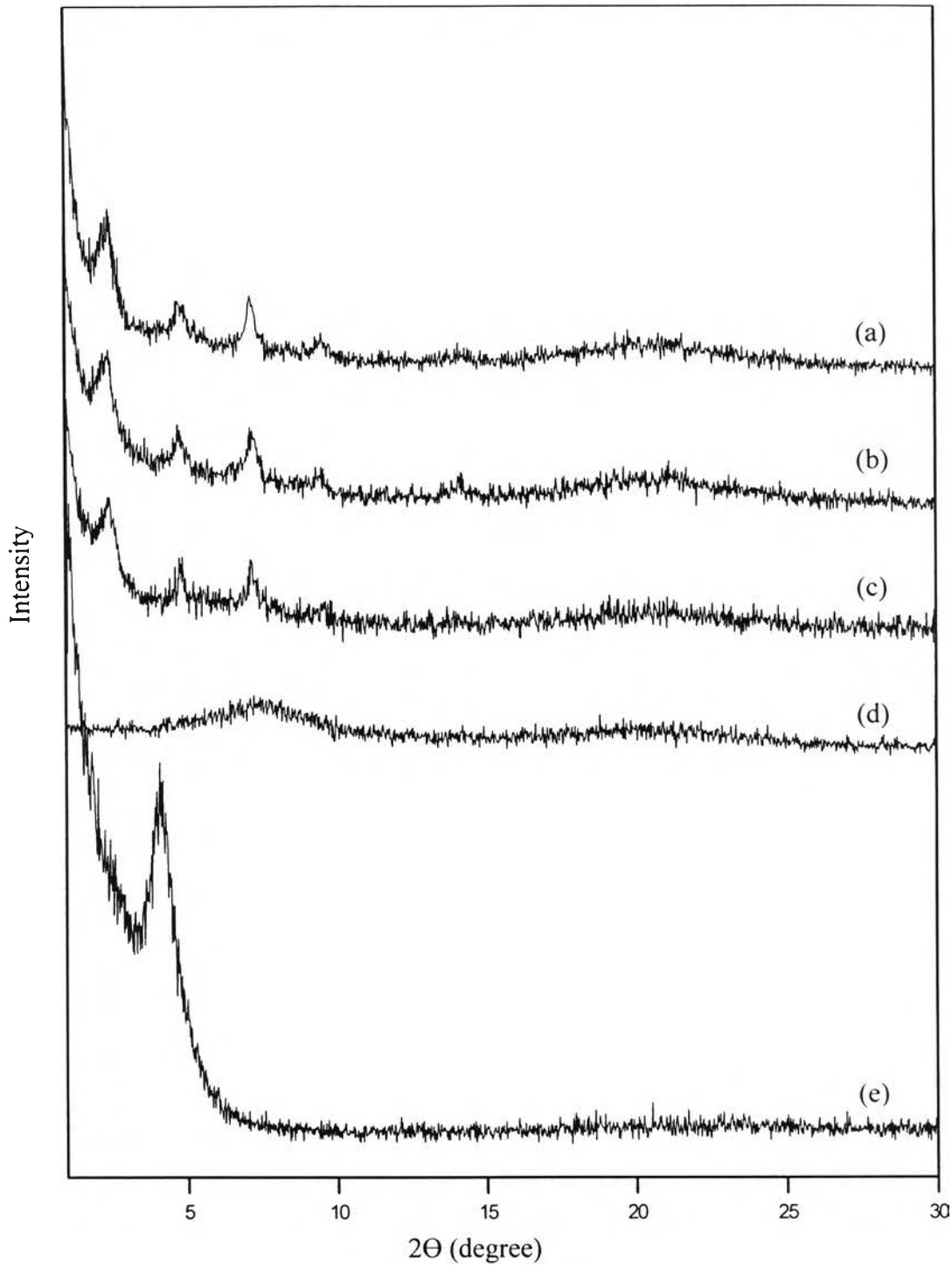

Figure 4.14 XRD patterns of (a) PB900Zn/BNH (5 wt%) (b) PB900Zn/BNH (3 wt%) (c) PB900Zn/BNH (1 wt%) (d) PB900Zn polyurethane (e) BNH organoclay

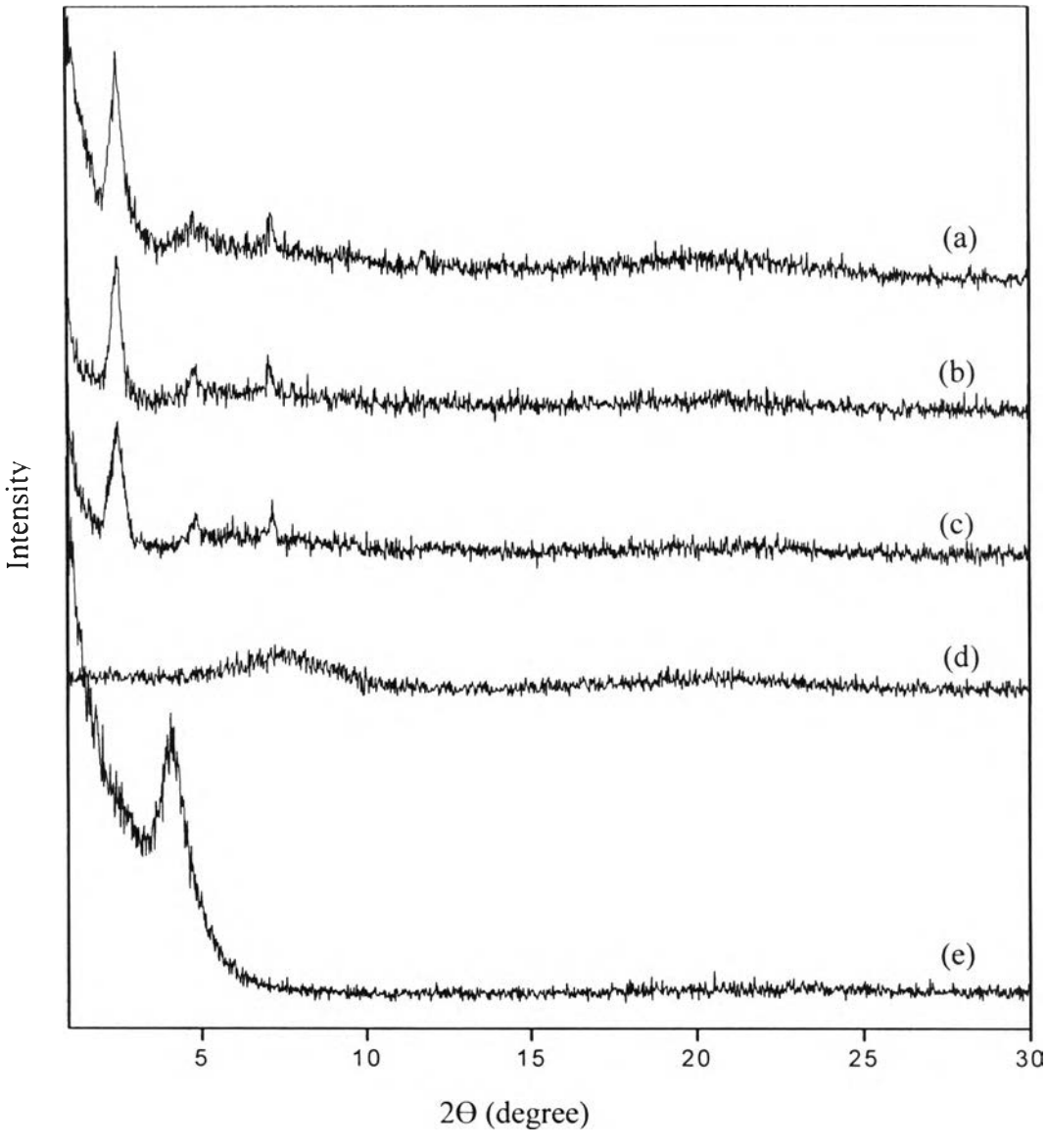

Figure 4.15 XRD patterns of (a) PP1000Zn/BNH (5 wt%) (b) PP1000Zn/BNH (3 wt%) (c) PP1000Zn/BNH (1 wt%) (d) PP1000Zn polyurethane (e) BNH organoclay

Table 4.6 XRD peak of organoclay, PB900Zn polyurethane and PB900Zn/BNH nanocomposites with various clay contents

Types	2θ (°)				$d_{001\text{-ave}}$
	d_{001}	d_{002}	d_{003}	d_{004}	
PB900Zn/BNH (5 wt%)	2.42	4.82	7.18	9.60	2.42
PB900Zn/BNH (3 wt%)	2.44	4.82	7.28	9.60	2.42
PB900Zn/BNH (1 wt%)	2.44	4.84	7.22	9.60	2.41
BNH organoclay	4.18	-	-	-	-

Table 4.7 d-spacing of organoclay, PB900Zn polyurethane and PB900Zn/BNH nanocomposites with various clay contents

Types	d-spacing of BNH organoclay (Å)				$d_{001\text{-ave}}$
	d_{001}	d_{002}	d_{003}	d_{004}	
PB900Zn/BNH (5 wt%)	36.2	18.2	12.2	9.2	36.5
PB900Zn/BNH (3 wt%)	36.2	18.3	12.1	9.2	36.5
PB900Zn/BNH (1 wt%)	36.5	18.3	12.3	9.2	36.7
BNH organoclay	21.1	-	-	-	-

Table 4.8 XRD peak of organoclay, PP1000Zn polyurethane and PP1000Zn/BNH nanocomposites with various clay contents

Types	2θ (°)				$d_{001\text{-ave}}$
	d_{001}	d_{002}	d_{003}	d_{004}	
PP1000Zn/BNH (5 wt%)	2.50	4.88	7.20	-	2.44
PP1000Zn/BNH (3 wt%)	2.50	4.84	7.18	-	2.44
PP1000Zn/BNH (1 wt%)	2.52	4.80	7.14	-	2.44
BNH organoclay	4.18	-	-	-	-

Table 4.9 d-spacing of organoclay, PP1000Zn polyurethane and PP1000Zn/BNH nanocomposites with various clay contents

Types	Interlayer spacing (Å)				$d_{001\text{-ave}}$
	d_{001}	d_{002}	d_{003}	d_{004}	
PP1000Zn/BNH (5 wt%)	35.0	18.4	12.3	-	36.2
PP1000Zn/BNH (3 wt%)	35.3	18.2	12.3	-	36.1
PP1000Zn/BNH (1 wt%)	35.3	18.1	12.2	-	36.1
BNH organoclay	21.1	-	-	-	-

4.4.3 TEM

The most direct measurement of the dispersion of these nanometer-scale silicates in the metal-containing PU can typically be found in the TEM micrographs of the cross section of polymer nanocompoites. TEM can further validate and complement the results of XRD. Figures 4.16-4.17 show the TEM photographs of the PB900Zn/BNH and PP1000Zn/BNH nanocomposites with 5 wt% of organoclay. The dark lines in Figures 4.16-4.17 represent intersection of OMH-BNH sheets while the grey part represents the metal-containing PU matrix. The intercalated domains having a collection of nearly parallel layered silicates. From Figure 4.16 (b), it can be evaluated that the basal spacing between layers exceeds 4.0 nm. Therefore, the TEM

result confirms the formation of intercalated structure of the metal-containing PU/BNH nanocomposites.

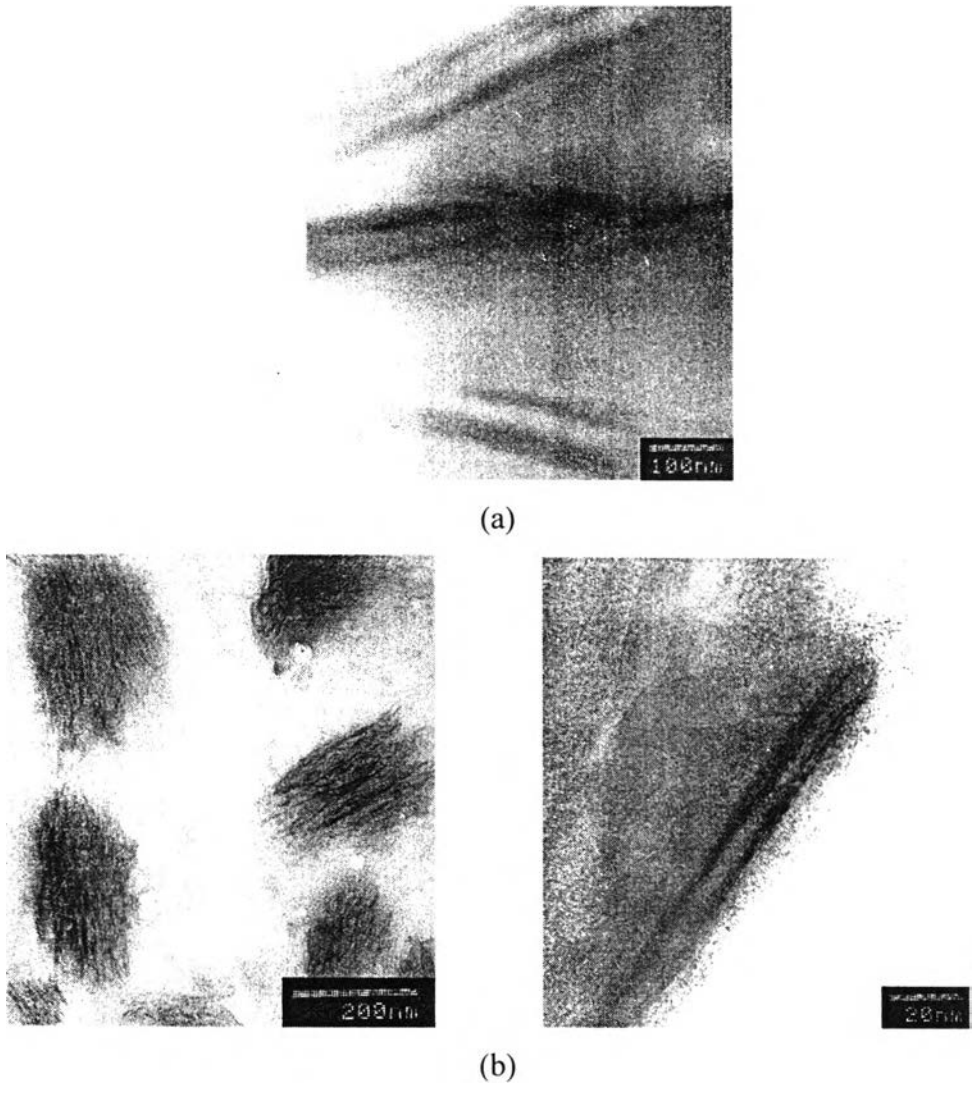

Figure 4.16 TEM micrographs of the (a) PB900Zn/BNH (1 wt%) (b) PB900Zn/BNH (5 wt%)

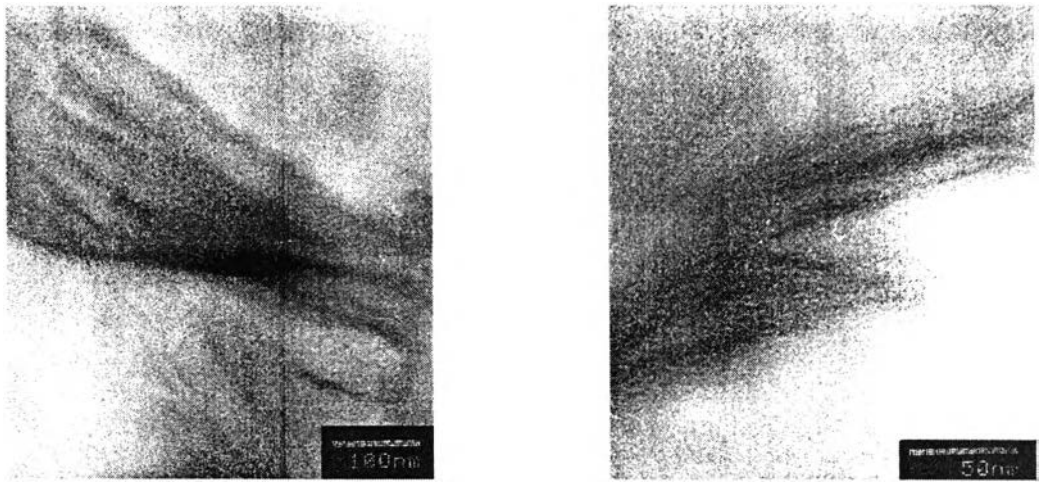

(a) (b)

Figure 4.17 TEM micrographs of the (a) PP1000Zn/BNH (1 wt%) (b) PP1000Zn/BNH (5 wt%)

4.5 Thermal Property

4.5.1 Investigation of Thermal Stability by TGA

Two nanocomposites chosen for this study were PB900Zn/BNH and PP1000Zn/BNH. The thermal degradation of pure metal-containing PU and its nanocomposites with different BNH organoclay loadings in nitrogen/air environment (50:50) was investigated by TGA. TGA thermograms of the polymers and nanocomposites are shown in Figures 4.18-4.19. Initial decomposition temperatures (IDTs) and % weight loss data are shown in Tables 4.10-4.11. The thermal stability of nanocomposites was not superior to that of the pure polymer at lower temperature. However, the % weight loss of the nanocomposites at high temperature was lower than that of the pure polymers in the range 430-1000 ^{o}C and 300-1000 ^{o}C for PB900Zn/BNH and PP1000Zn/BNH nanocomposites, respectively. The % weight loss in this high temperature range decreased with increase in the amount of organoclay.

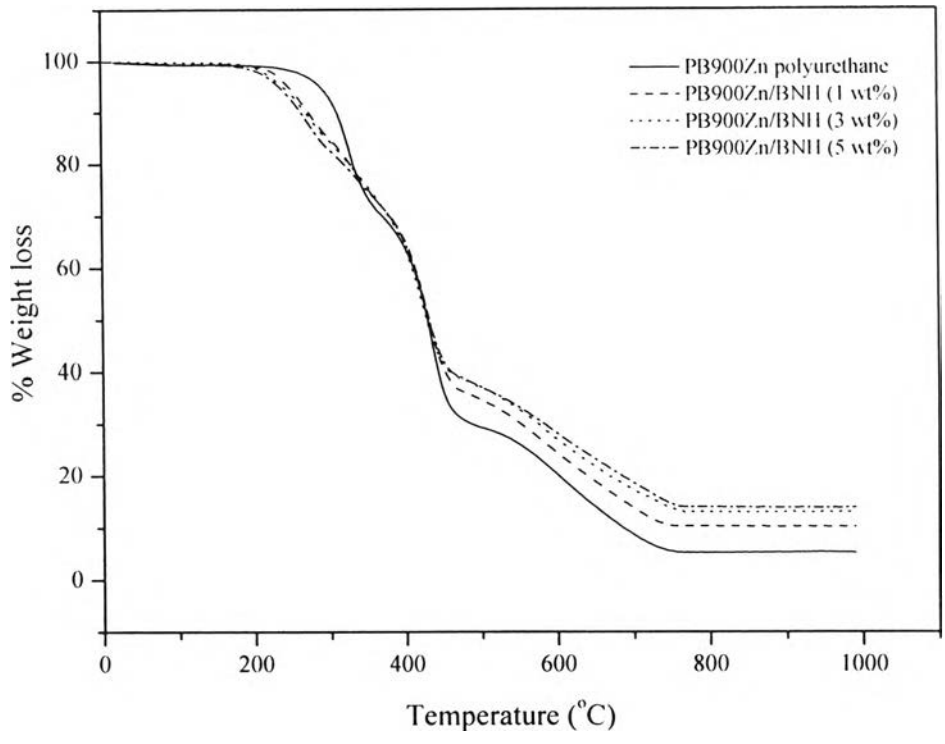

Figure 4.18 TGA thermogram of PB900Zn polyurethane and PB900Zn/BNH nanocomposites with various clay contents

Table 4.10 Weight loss percentages of PB900Zn polyurethane and PB900Zn/BNH nanocomposites with various clay contents

Polymer	IDTs	% Weight loss at different temperatures					
		300	400	500	600	700	800
PB900Zn polyurethane	237	6	36	70	80	91	95
PB900Zn/BNH (1 wt%)	204	15	35	65	76	86	90
PB900Zn/BNH (3 wt%)	202	15	36	63	73	83	87
PB900Zn/BNH (5 wt%)	188	17	35	63	72	81	86

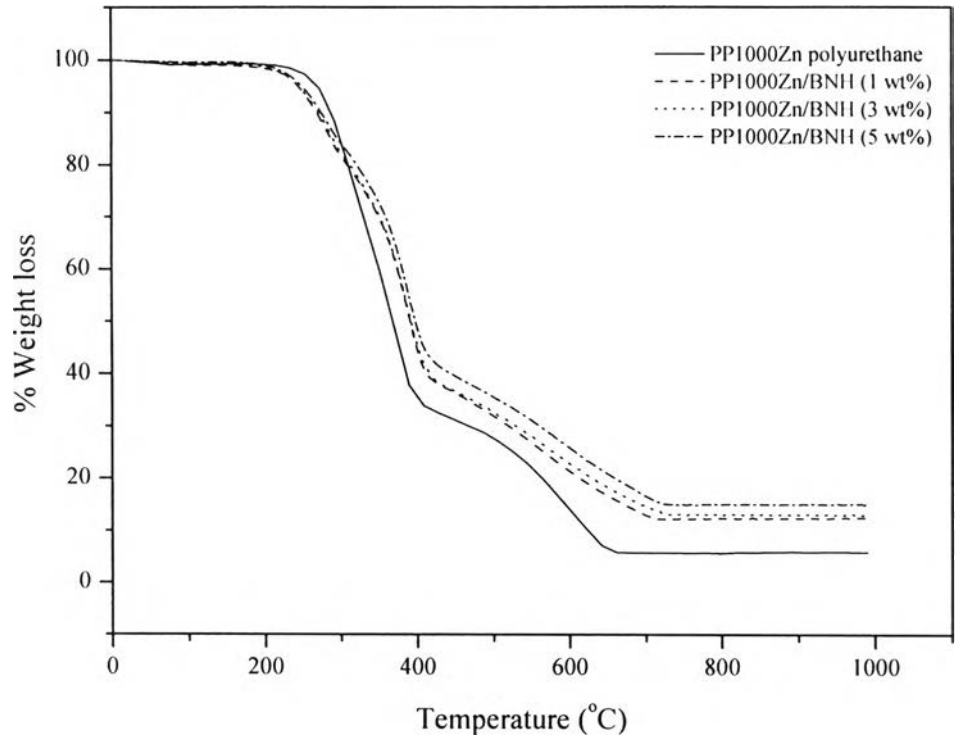

Figure 4.19 TGA thermogram of PP1000Zn polyurethane and PP1000Zn/BNH nanocomposites with various clay contents

Table 4.11 Weight loss percentages of PP1000Zn polyurethane and PP1000Zn/BNH nanocomposites with various clay contents

Polymer	IDTs	% Weight loss at different temperatures					
		300	400	500	600	700	800
PP1000Zn polyurethane	227	15	65	72	86	94	94
PP1000Zn/BNH (1 wt%)	208	17	54	67	78	86	87
PP1000Zn/BNH (3 wt%)	190	17	54	67	77	85	87
PP1000Zn/BNH (5 wt%)	186	15	51	64	74	83	85

The above TGA results indicated that there is interaction between metal-containing PU chain and surface of organoclay because both of them contain polar

species. Figure 4.20 illustrates a possible interaction between the polymer chain and organocaly surface.

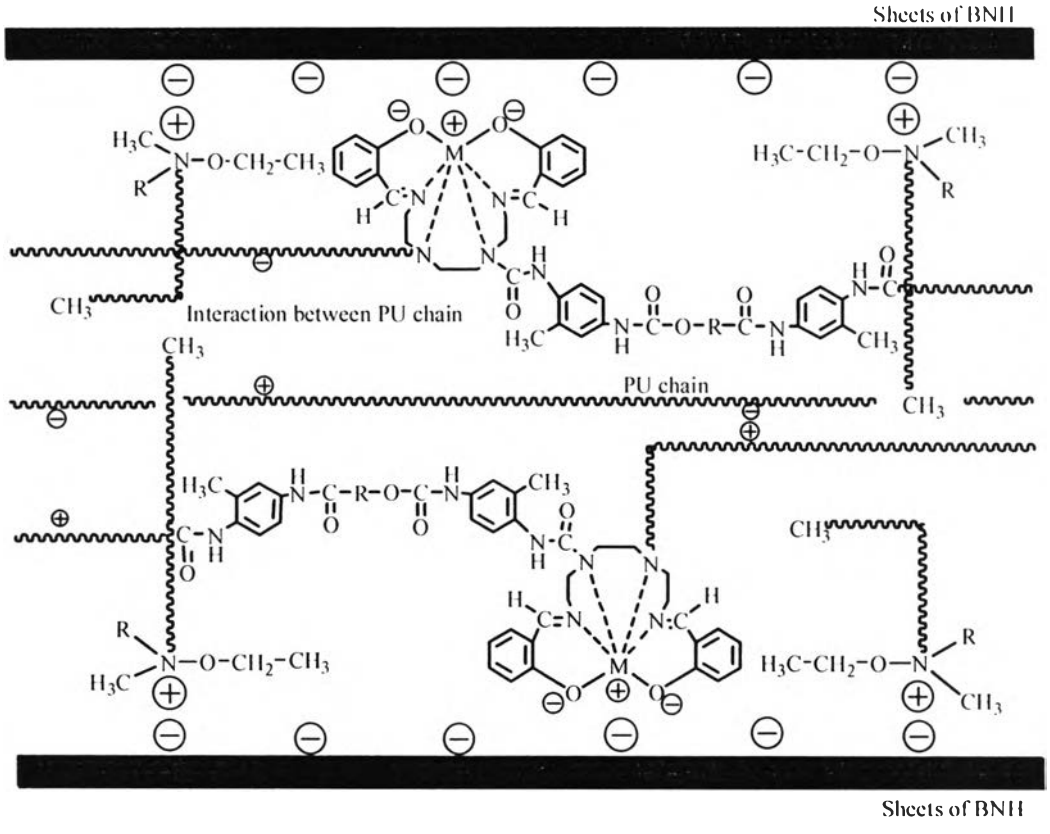

Figure 4.20 Proposed interaction between polymer chain and organoclay surface

TGA results showed that the IDTs of the nanocomposites was lower than those of pure polymers. This might be due to the thermal decomposition of the OMH quaternary ammonium salt that was employed in the modification of the surface of clay. Hofmann degradation of OMH quaternary ammonium salt could take place [40] as shown in Scheme 4.1. Trace HCl resulted from Hofmann degradation could act as catalyst for first stage decomposition of the metal-containing PU. Therefore, the introduction of quaternary ammonium salts in the nanocomposites could reduce their IDTs.

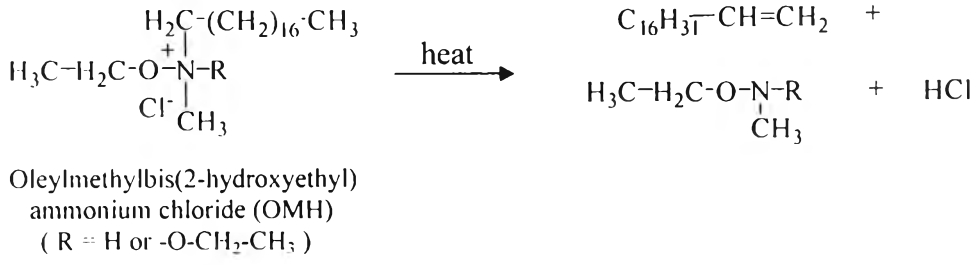

Oleylmethylbis(2-hydroxyethyl) ammonium chloride (OMH) (R = H or -O-CH_2-CH_3)

Scheme 4.1 Hofmann degradation of OMH quaternary ammonium salt

4.5.2 Flame Retardancy

The flammability behavior of pure metal-containing PU and the metal-containing PU/BNH nanocomposites was evaluated by LOI value measurement. The LOI values of samples in this experiment are listed in Table 4.12. The LOI values increased with an increase in organoclay content of the nanocomposite, implying that the flame retardancy of the metal-containing PU polymer was improved by the presence of organoclay in the metal-containing PU matrix.

Table 4.12 LOI data of the metal-containing polyurethanes and their corresponding nanocomposites

Polymer	LOI	Polymer	LOI
PB900Zn polyurethane	23.0	PP1000Zn polyurethane	23.6
PB900Zn/BNH (1 wt%)	24.3	PP1000Zn/BNH (1 wt%)	24.5
PB900Zn/BNH (3 wt%)	24.4	PP1000Zn/BNH (3 wt%)	25.2
PB900Zn/BNH (5 wt%)	25.4	PP1000Zn/BNH (5 wt%)	25.6